Table 2
Masked samples used to assess the developed models[a].

Sample name	Male/Female	Core body temperature [°C]
N 1	F	36.8
N 2	M	36.5
N 3	F	36.4
N 4	M	36.0
N 5	F	36.3
N 44	F	36.2
N 45	M	36.3
N 46	M	36.4
N 47	M	36.4
N 48	M	36.7
I 1	M	36.7
I 2	F	36.3
I 3	F	36.3
I 5	F	36.4
I 6	F	36.0
I 48	F	36.6
I 49	F	36.7
I 50	M	36.7
I 51	F	36.9
I 52	F	36.9
R 1	M	36.4
R 2	F	36.1
R 4	F	36.2
R 5	F	36.4
R 6	F	36.9
R 7	F	36.8
R 8	F	37.0
R 9	F	36.9
R 10	F	37.0
R 12	F	36.7
R 13	F	36.7
R 14	F	36.7
R 17	M	36.9
R 18	F	36.9
R 19	F	36.9
R 20	M	36.9
R 21	F	36.8
R 22	F	36.8
R 23	M	36.8
R 24	M	36.9
R 25	F	37.1
R 26	M	36.4

[a] N1-N48 are non-influenza samples, while I1-I52 are influenza samples. R1-R26 are RSV-infected samples. Core body temperatures of non-influenza, influenza, and RSV-infected patients at the time when nasal aspirates were collected from patients are shown.

were separated in multivariate space, providing validation for this class separation (Fig. 2A). In a further test, masked samples were subjected to Vis-NIR spectroscopy, and the spectral data were applied to the the PCA and SIMCA models. Discrimination of the masked nasal aspirate samples between influenza and non-influenza patients was attained using the PCA and SIMCA models of Vis-NIR spectra (Figs. 1B, 2B). Furthermore, PCA showed some discrimination of the masked samples among non-influenza, influenza, and RSV-infected patients. SIMCA correctly predicted 29 of 30 (96.67%) non-influenza samples, and 30 of 30 (100%) influenza samples (Table 4); however, the 66 samples from RSV-infected patients were predicted as 33 (50%) non-influenza and 33 (50%) influenza (Table 4), suggesting that discrimination between RSV infection and influenza or non-influenza was difficult.

The spectral information modeled by PCA or SIMCA can be inferred from the corresponding "loadings" or "discriminating power", respectively. Concerning PC1, the loadings showed a negative broad peak from 700 to 950 nm (Fig. 1C). The PC2 loadings showed a negative peak around 950 nm, and a positive peak around 1030 nm. The PCA loadings were generally consistent with the discriminating power of the SIMCA model, except that the latter had an additional 640-nm peak in discriminating power (Fig. 2C). The most prominent discriminating power, which represents independent variables (wavelengths) important in discriminating between the two classes
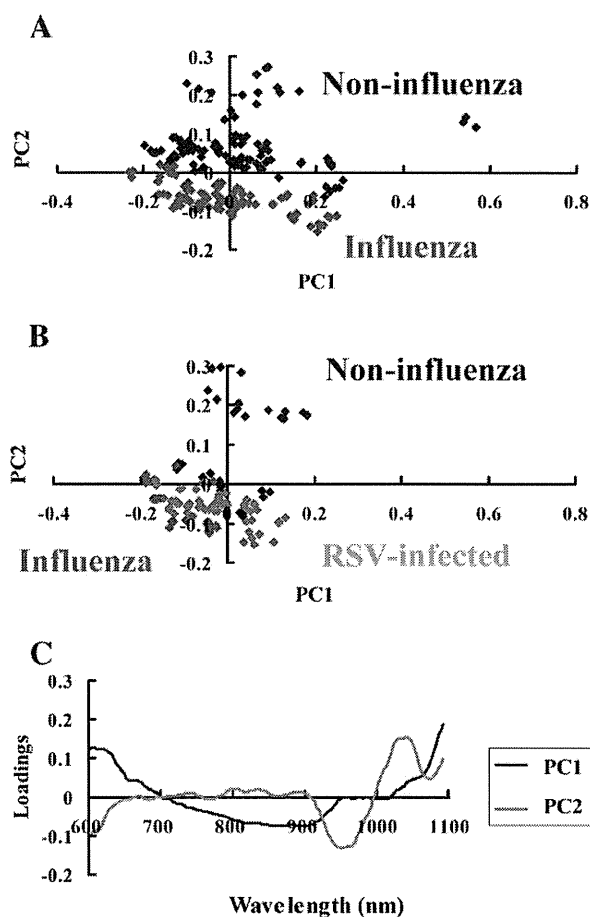

Fig. 1. Principal component analysis (PCA) (first 2 principal components) of visible and near-infrared (Vis-NIR) calibration and prediction of influenza diagnosis. Nasal aspirates from non-influenza patients, influenza patients, and patients infected with respiratory syncytial virus (RSV) were subjected to Vis-NIR spectroscopy. The spectral data were pre-processed and subjected to PCA calibration modeling to develop a multivariate model to diagnose influenza. (A,B) PCA score plot of the first principal component (PC1) versus the second principal component (PC2) for the Vis-NIR spectra of test samples comprising 35 non-influenza and 34 influenza patients (A) and that of the spectra of masked samples comprising 10 non-influenza patients, 10 influenza patients, and 22 RSV-infected patients (B). The plots demonstrated discrimination between non-influenza (blue diamonds) and influenza (red diamonds) patients, whereas RSV-infected patients (green diamonds) showed some overlap with non-influenza and influenza patients and were located between the 2 groups. (C) PC1 (blue line) and PC2 (red line) loadings of the PCA.

(influenza and non-influenza), were the sharp peaks at 850, 950, and 1030 nm and the broad peaks at around 660–740 nm (Fig. 2C).

The peak around 950 nm was close to a water band [13]. The peak near 850 nm was previously assigned to a C-H aromatic group [13,30], whereas that near 1030 nm could be assigned to alcohols [13,30]. The peaks around 660–740 nm are also related to both alcohols and C-H aromatic groups [13,30,31]. However, further studies will be necessary to accurately perform band assignment for the peaks that are important for PCA loadings and SIMCA discriminating power. Further information obtained from detailed analysis of the Vis-NIR spectra of nasal aspirates may make significant contributions

Table 3
Prediction of non-influenza and influenza among test samples by the SIMCA model of influenza diagnosis.

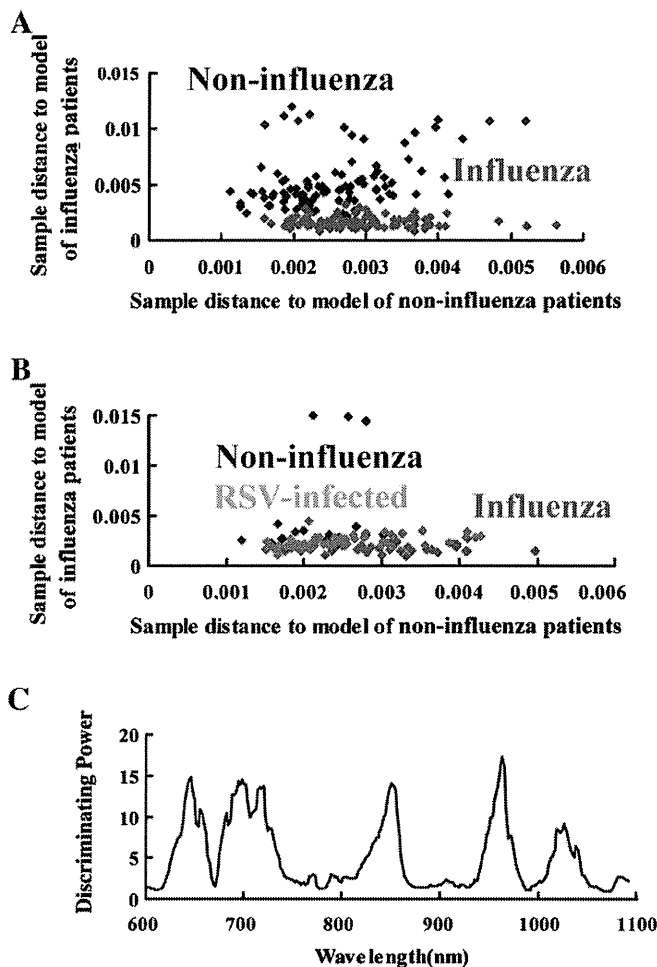| Test sample	Predicted non-influenza	Predicted influenza	No match
Actual non-influenza	100	5	0
Actual influenza	7	95	0

Fig. 2. Soft modeling of class analogy (SIMCA) of Vis-NIR calibration and prediction of influenza diagnosis. Vis-NIR spectral data of nasal aspirates from non-influenza and influenza patients were pre-processed and subjected to SIMCA calibration modeling to develop a multivariate model to diagnose influenza. (A) Coomans plot of SIMCA demonstrating that the non-influenza class (blue diamonds) and influenza patient class (red diamonds) of test samples showed separated multivariate space. (B) Masked samples from the non-influenza class (blue diamonds) and influenza class (red diamonds) demonstrated discrimination, but each showed some overlap with the RSV-infected class (green diamonds). (C) Discriminating power of the SIMCA calibration model.

changes in the Vis-NIR spectra of nasal aspirates from influenza and RSV patients. In contrast, the difference in core body temperatures between non-influenza and influenza patients at the time when nasal aspirates were collected from patients was not significant, whereas the core body temperatures of RSV-infected patients were significantly higher than those of non-influenza and influenza patients (Supplemental Fig. 1). In future studies, it would be interesting to follow patients through the course of disease to see if any of these parameters might change and correlate or act as predictors of outcome. In addition, further fractionation of the nasal aspirate (e.g. into soluble and particulate fractions) may increase the power to discriminate influenza from RSV-infection (or other) samples as part of future efforts.

Currently, there are various diagnostic methods for influenza such as immunochromatography, reverse transcription (RT)-polymerase chain reaction (PCR), and real-time RT-PCR. The price of a single immunochromatography test is $10, and the handling time required for this test is 30 min. Because immunochromatography can detect only high concentrations of virus, other additional methods such as RT-PCR should be combined for high-sensitivity detection of influenza virus. The cost of a single real-time or normal RT-PCR is $5–10 ($10–20 for a test in duplicate) and the required time is 6 h. Furthermore, the price of a PCR instrument is > $8000. In comparison to these conventional methods, the Vis-NIR spectroscopy method requires a similar time (4–5 h) to PCR to develop a calibration model. Furthermore, the Vis-NIR spectrometer is expensive (> $10,000), similar to the PCR instrument. After development of the calibration model, however, the Vis-NIR spectroscopy method is rapid (<1 min for measurement) and requires no regents for the analysis. The price of a single measurement is only the cost of the electricity and plastic measurement tubes. Therefore, if a successful calibration model could be developed, the cost and efficiency of Vis-NIR spectroscopy as a diagnostic method would be excellent. Thus, combinational use of Vis-NIR spectroscopy may compensate for some of the weaker points of conventional diagnostic methods.

In summary, the present findings indicate that, combined with chemometrics analysis, the Vis-NIR spectra of nasal aspirates can distinguish between influenza patients and non-influenza patients. The current study has limitations, including a small number of patients restricted to the Japanese population, which means that the spectral data from nasal aspirates is representative. Moreover, discrimination between influenza virus infection and RSV infection was difficult, and further studies will be necessary to achieve this discrimination by Vis-NIR spectroscopy. In addition, it should be examined whether this method can be used for populations of different ethnicities and ages. There are also other limitations including how to differentiate different types of influenza, and how to improve the specificity of diagnosis by reducing the interference from other viruses or chemicals with similar spectra. Band assignment to determine the peaks important in PCA loadings and SIMCA discriminating power would provide clues to a more reliable and specific diagnostic method for influenza. Taking the results altogether, however, this approach deserves further evaluation as a potential novel strategy for instrumental, objective, and cost-effective diagnosis of influenza. Finally, although the present study showed the possibility of Vis-NIR spectroscopy using nasal aspirates, non-invasive approaches to the diagnosis of influenza using Vis-NIR spectra directly collected from the body without collecting nasal fluid are also interesting [14,36].

Supplementary data to this article can be found online at http://dx.doi.org/10.1016/j.cca.2012.08.022.

not only to the diagnosis but also to our understanding of the pathogenesis of influenza in the nasal mucosal region. In general, cytokines and chemokines induced by influenza virus infection may cause a change in constituents or activation of lymphocytes in the nasal fluid [32–34], resulting in the spectral changes observed in the nasal aspirates. Activation of lymphocytes subsequently may induce various changes, such as modulation of protein expression and movement of surrounding cells. Such changes caused by the influenza virus may be similar to those caused by RSV, but may differ from those occurring in non-influenza infection [35], resulting in similar

Table 4
Prediction of non-influenza, influenza, and RSV-infection among masked samples by the SIMCA model of influenza diagnosis.

Masked sample	Predicted non-influenza	Predicted influenza	No match
Actual non-influenza	29	1	0
Actual influenza	0	30	0
Actual RSV-infected	33	33	0

References

[1] WHO. Available from:http://www.who.int/mediacentre/factsheets/2003/fs211/en/; 2003.

[2] Spackman E. A brief introduction to the avian influenza virus. Methods Mol Biol 2008;436:1-6.

[3] Palese P, Shaw ML. Orthomyxoviridae: the viruses and their replication. In: Knipe DM, Howley PM, editors. Fields Virology. Philadelphia: Lippincott Williams & Wilkins; 2006. p. 1647-89.

[4] Nicholson KG, Webster RG, Hays AJ. Textbook of influenza. Oxford: Blackwell Science; 1998.

[5] Fairchok MP, Martin ET, Chambers S, Kuypers J, Behrens M, Braun LE, Englund JA. Epidemiology of viral respiratory tract infections in a prospective cohort of infants and toddlers attending daycare. J Clin Virol 2010;49:16-20.

[6] Dagnelie CF, Bartelink ML, van der Graaf Y, Goessens W, de Melker RA. Towards a better diagnosis of throat infections (with group A beta-haemolytic streptococcus) in general practice. Br J Gen Pract 1998;48:959-62.

[7] Ebihara T, Endo R, Kikuta H, Ishiguro N, Ishiko H, Hara M, et al. Human metapneumovirus infection in Japanese children. J Clin Microbiol 2004;42: 126-32.

[8] Sugaya N, Mitamura K, Nirasawa M, Takahashi K. The impact of winter epidemics of influenza and respiratory syncytial virus on paediatric admissions to an urban general hospital. J Med Virol 2000;60:102-6.

[9] Barenfanger J, Drake C, Leon N, Mueller T, Troutt T. Clinical and financial benefits of rapid detection of respiratory viruses: an outcomes study. J Clin Microbiol 2000;38:2824-8.

[10] Dwyer DE, Smith DW, Catton MG, Barr IG. Laboratory diagnosis of human seasonal and pandemic influenza virus infection. Med J Aust 2006;185:S48-53.

[11] Chartrand C, Leeflang MM, Minion J, Brewer T, Pai M. Accuracy of rapid influenza diagnostic tests: a meta-analysis. Ann Intern Med 2012;156:500-11.

[12] Ciurczak EW, Drennen JK. Pharmaceutical and medical applications of near-infrared applications (pratical spectroscopy). New York: Marcel Dekker Inc.; 2002.

[13] Osborne BG, Fearn T. Near-infrared spectroscopy in food analysis. UK: Longman Scietific & Technical; 1986.

[14] Sakudo A, Suganuma Y, Kobayashi T, Onodera T, Ikuta K. Near-infrared spectroscopy: promising diagnostic tool for viral infections. Biochem Biophys Res Commun 2006;341:279-84.

[15] Jolliffe IT. Principal Component Analysis. New York: Springer; 2002.

[16] Wold S. Pattern recognition by means of disjoint principal components models. Pattern Recogn 1976;8:127-39.

[17] Barnes RJ, Dhanoa MS, Lister SJ. Standard normal variate transformation and de-trending of near-infrared diffuse reflectance spectra. Appl Spectrosc 1989;43: 772-7.

[18] Savitzky A, Golay MJE. Smoothing and differentiation of data by simplified least-squares procedures. Anal Chem 1964;36:1627-39.

[19] Coomans D, Broeckaert I, Derde MP, Tassin A, Massart DL, Wold S. Use of a microcomputer for the definition of multivariate confidence regions in medical diagnosis based on clinical laboratory profiles. Comput Biomed Res 1984;17:1-14.

[20] Gillissen A, Hoffken G. Early therapy with the neuraminidase inhibitor oseltamivir maximizes its efficacy in influenza treatment. Med Microbiol Immunol 2002;191: 165-8.

[21] Sakudo A, Tsenkova R, Onozuka T, Morita K, Li S, Warachit J, et al. A novel diagnostic method for human immunodeficiency virus type-1 in plasma by near-infrared spectroscopy. Microbiol Immunol 2005;49:695-701.

[22] Sakudo A, Kuratsune H, Kobayashi T, Tajima S, Watanabe Y, Ikuta K. Spectroscopic diagnosis of chronic fatigue syndrome by visible and near-infrared spectroscopy in serum samples. Biochem Biophys Res Commun 2006;345:1513-6.

[23] Nojima J, Sakudo A, Hakariya Y, Kuratsune H, Watanabe Y, Kanakura Y, et al. Spectroscopic diagnosis of anti-phospholipid antibodies by visible and near-infrared spectroscopy in SLE patients' plasma samples. Biochem Biophys Res Commun 2007;362:522-4.

[24] Kato YH, Matsunaga H, Sakudo A, Ikuta K. Visible and near-infrared spectral changes in plasma of psychiatric patients. Int J Mol Med 2008;22:513-9.

[25] Kobayashi T, Kato YH, Tsukamoto M, Ikuta K, Sakudo A. Portable visible and near-infrared spectrophotometer for triglyceride measurements. Int J Mol Med 2009;23:75-9.

[26] Sakudo A, Suganuma Y, Sakima R, Ikuta K. Diagnosis of HIV-1 infection by near-infrared spectroscopy: analysis using molecular clones of various HIV-1 subtypes. Clin Chim Acta 2012;413:467-72.

[27] Sakudo A, Kato YH, Tajima S, Kuratsune H, Ikuta K. Visible and near-infrared spectral changes in the thumb of patients with chronic fatigue syndrome. Clin Chim Acta 2009;403:163-6.

[28] Sakudo A, Kuratsune H, Kato YH, Ikuta K. Visible and near-infrared spectra collected from the thumbs of patients with chronic fatigue syndrome for diagnosis. Clin Chim Acta 2012.

[29] Sakudo A, Kato YH, Kuratsune H, Ikuta K. Non-invasive prediction of hematocrit levels by portable visible and near-infrared spectrophotometer. Clin Chim Acta 2009;408:123-7.

[30] Williams P, Norris K. Near-Infrared Technology in the Agricultural and Food Industories. St. Paul: Academic Association of Cereal Chemists; 1987.

[31] Workman J, Weyer L. Practical Guide to Interpretative Near-Infrared Spectroscopy. New York: CRC Press; 2008.

[32] Eccles R. Understanding the symptoms of the common cold and influenza. Lancet Infect Dis 2005;5:718-25.

[33] Brown DM, Roman E, Swain SL. CD4 T cell responses to influenza infection. Semin Immunol 2004;16:171-7.

[34] Julkunen I, Melen K, Nyqvist M, Pirhonen J, Sareneva T, Matikainen S. Inflammatory responses in influenza A virus infection. Vaccine 2000;19(Suppl. 1):S32-7.

[35] Welliver RC. Respiratory syncytial virus and other respiratory viruses. Pediatr Infect Dis J 2003;22:S6-S10.

[36] Sakudo A, Baba K, Ikuta K. Analysis of Vis-NIR spectra changes to measure the inflammatory response in the nasal mucosal region of influenza A and B virus-infected patients. J Clin Virol, in press, http://dx.doi.org/10.1016/j.jcv.2012.08.015.

ORIGINAL PAPER

Discovery of novel low-molecular-weight HIV-1 inhibitors interacting with cyclophilin A using in silico screening and biological evaluations

Yu-Shi Tian · Chris Verathamjamras ·
Norihito Kawashita · Kousuke Okamoto ·
Teruo Yasunaga · Kazuyoshi Ikuta ·
Masanori Kameoka · Tatsuya Takagi

Abstract Cyclophilin A has attracted attention recently as a new target of anti-human immunodeficiency virus type 1 (HIV-1) drugs. However, so far no drug against HIV-1 infection exhibiting this mechanism of action has been approved. To identify new potent candidates for inhibitors, we performed in silico screening of a commercial database of more than 1,300 drug-like compounds by using receptor-based docking studies. The candidates selected from docking studies were subsequently tested using biological assays to assess anti-HIV activities. As a result, two compounds were identified as the most active. Specifically, both exhibited anti-HIV activity against viral replication at a low concentration and relatively low cytotoxicity at the effective concentration inhibiting viral growth by 50 %. Further modification of these molecules may lead to the elucidation of potent inhibitors of HIV-1.

Keywords Drug design · In silico screening · Anti-HIV · Cyclophilin A · Inhibitor

Yu-Shi Tian and Chris Verathamjamras contributed equally to this work.

Y.-S. Tian · N. Kawashita · K. Okamoto · T. Takagi (✉)
Graduate School of Pharmaceutical Sciences, Osaka University,
1-6 Yamadaoka,
Suita, Osaka 565-0871, Japan
e-mail: ttakagi@phs.osaka-u.ac.jp

C. Verathamjamras · M. Kameoka (✉)
Thailand-Japan Research Collaboration Center on Emerging
and Re-emerging Infections (RCC-ERI),
Building 10, Department of Medical Sciences,
Ministry of Public Health, Tiwanon Rd.,
Muang, Nonthaburi 11000, Thailand
e-mail: mkameoka@biken.osaka-u.ac.jp

N. Kawashita · T. Yasunaga · T. Takagi
Genome Information Research Center, Research Institute for
Microbial Diseases, Osaka University,
3-1 Yamadaoka,
Suita, Osaka 565-0871, Japan

K. Ikuta · M. Kameoka
Department of Virology, Research Center for Infectious Disease
Control, Research Institute for Microbial Diseases,
Osaka University,
3-1 Yamadaoka,
Suita, Osaka 565-0871, Japan

Introduction

Cyclophilin A (CypA) was discovered originally as the receptor of the immunosuppressive drug cyclosporin A (CsA)—a molecule exhibiting multiple biological functions. The formation of complexes between CypA and CsA, which is an 11-mer cyclic peptide isolated from the fungus *Tolypocladium inflatum*, allows CypA to interact with calcineurin, reduce the production of interferon γ and interleukin-2, and exert immunosuppressive effects [1]. CypA is one of 15 known human cyclophilins, and can catalyze cis–trans isomerization in peptide bonds containing proline via its peptidyl prolyl isomerase (PPIase) activity. Recently, it was reported that CypA interacts with the NS5A and NS5B parts of hepatitis C virus polymerase [2, 3], the nucleocapsid protein of the SARS coronavirus [4], and the capsid (CA) protein of human immunodeficiency virus type 1 (HIV-1) [5]. These multiple functions make CypA an attractive target for drug development.

In addition to CsA, the natural product sanglifehrin A [6] and several peptide analogs [7] were reported to be active inhibitors of CypA. Recently, to decrease HIV-1 infectivity by disrupting the interaction of CypA with CA, several small molecules have been developed [8, 9]. However,

🕏 Springer

new drugs against HIV-1 infection exhibiting this mechanism of action have not yet been approved.

Nevertheless, there are several published reports of structural information regarding to the binding modes of CypA and CA fragments [10], CsA [11], or small peptides [12], and the available information suggests the potential applicability of in silico inhibitor screening and design for elucidating potential inhibitors. Here, we screened a small database of 1,377 small-molecular-weight compounds. A total of 29 compounds was selected according to docking scores. Together with two commercial positive control compounds, these 29 selected compounds were tested using biological assays. Finally, two compounds were identified as potent anti-HIV candidates, displaying acceptable cellular toxicity.

Materials and methods

Small molecular database for virtual screening

The structures of 1,377 low-molecular-weight compounds in a chemical structure data (SD) file format were obtained from ChemGenesis (http://www.all-chemy.com/), who supplied all the compound samples in the file. This SD file was converted into Molecular Operating Environment (MOE; Chemical Computing Group, Montreal, Canada) database format, and energy optimization of each molecule was performed under the MMFF94x forcefield using the MOE
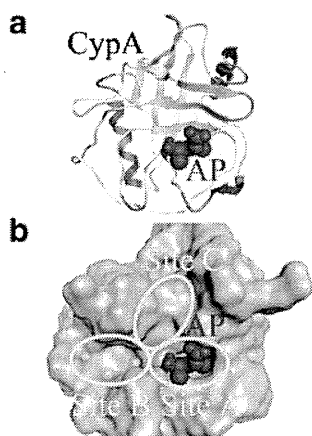

Fig. 2 Comparison of the re-docked conformation of AP with the crystallographic conformation in the CypA/AP complex. *Blue* Redocked conformation, *red* crystallographic conformation. The root mean squared deviation (RMSD) between the two conformations was as low as 0.261 Å. The surface of the receptor is colored according to lipophilicity. *Green* Hydrophobic areas, *pink* hydrophilic areas

software package. The descriptors of molecular weight, lip_violation, lip_druglike [13], and diameter were calculated and typed into the fields of the database to confirm the basic properties of the compounds in the database.

Preparation of ligands and protein

The 1.64-Å resolution crystallographic data of CypA in complex with the dipeptide alanine-proline (AP; PDB entry 2CYH) [12] was obtained from the Brookhaven Protein Data Bank (http://www.pdb.org/pdb). This co-crystallized structure was used in preliminary studies to determine whether the docking parameters used were appropriate, and the structure of CypA within the structure was used as a receptor for screening the Allchemy database. In the present study, the "MOE dock" program was used to perform all the screening procedures. The Protonate3D module in MOE was used to assign ionization states, and to position hydrogen atoms into

Fig. 1a,b The structure of receptor cyclophilin A (CypA) and its binding sites. **a** Representation of the dipeptide alanine-proline (AP, *red*) inside the CypA active site cavity. CypA adopts an eight-stranded antiparallel beta barrel structure, and AP is buried deeply in one of the cavities on the surface of CypA. The structure was obtained from 2CYH.pdb, and the figure was created by Molecular Operating Environment (MOE; Chemical Computing Group, Montreal, Canada) software. **b** Three docking sites on the surface of CypA. *Site A* is also known as the CypA MVA11-binding pocket, and AP also binds here. *Site B* is a hydrophobic pocket that is also known as the CypA Abu2-binding pocket. Above these two sites, there is some space, which we call *Site C* in this paper
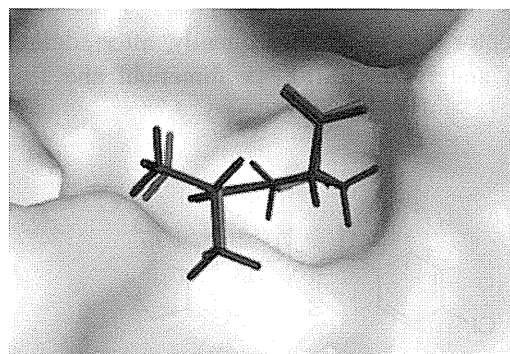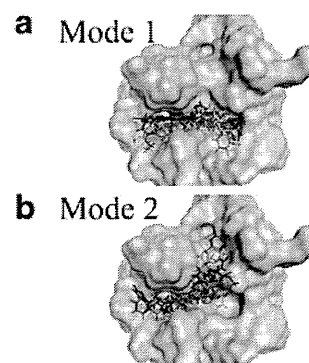

Fig. 3a,b Control compounds D4 and FD8 and 29 selected compounds docked into the surface sites of CypA. **a** Mode 1: lowest scored pose of each compound covered the region of Site A and Site B. **b** Mode 2: lowest scored pose of each compound docked into Site B and Site C, but not Site A

the receptor molecule. Subsequently, after adding partial charges under the MMFF94x forcefield and fixing the

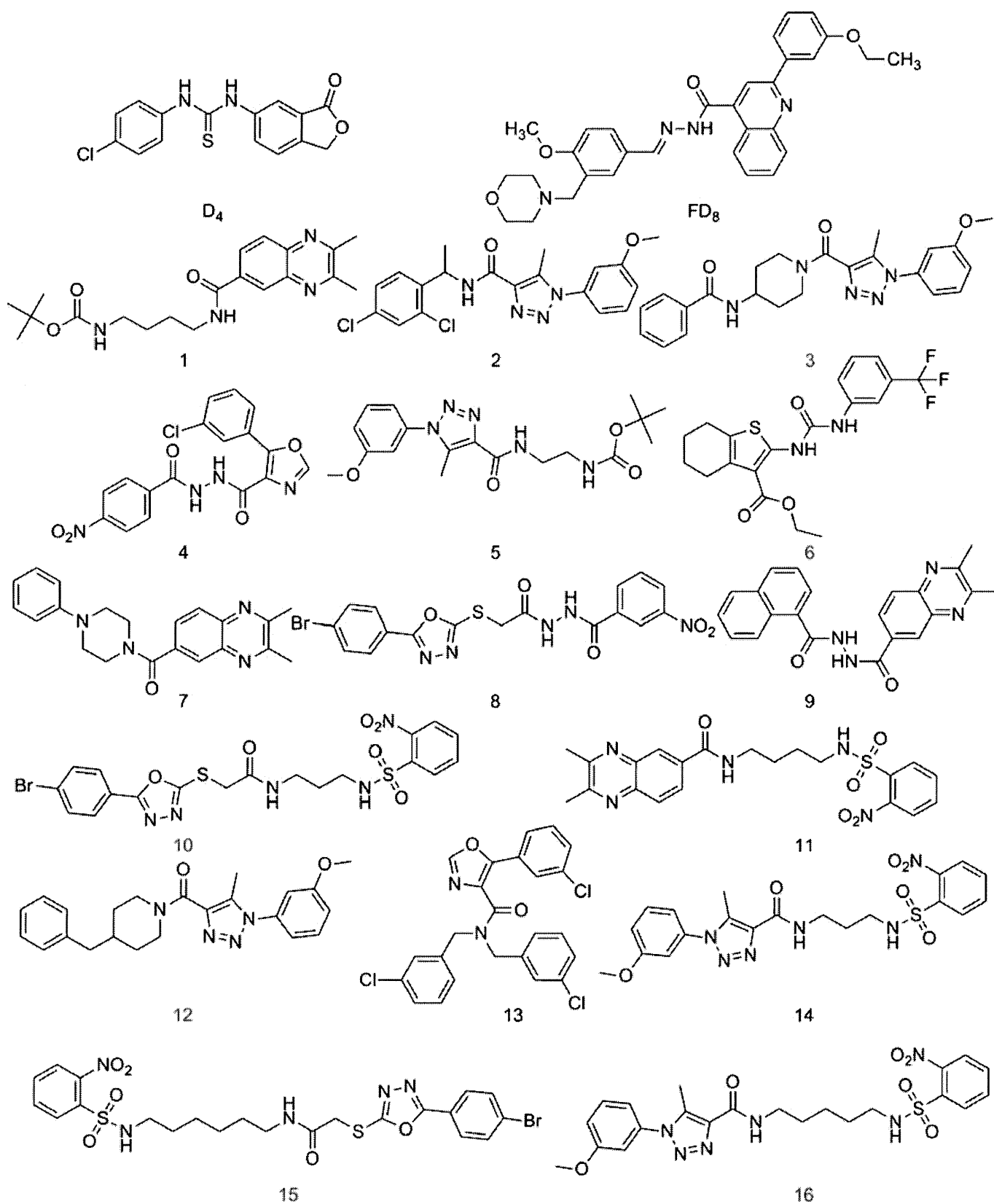backbone atoms, energy minimization of the receptor was performed.

Fig. 4 Structures of compounds selected from the docking studies and the control compounds (D4 and FD8). The identifiers of compounds docking in Mode 1 poses are in *black*, and those of compounds docking in Mode 2 poses are in *blue*
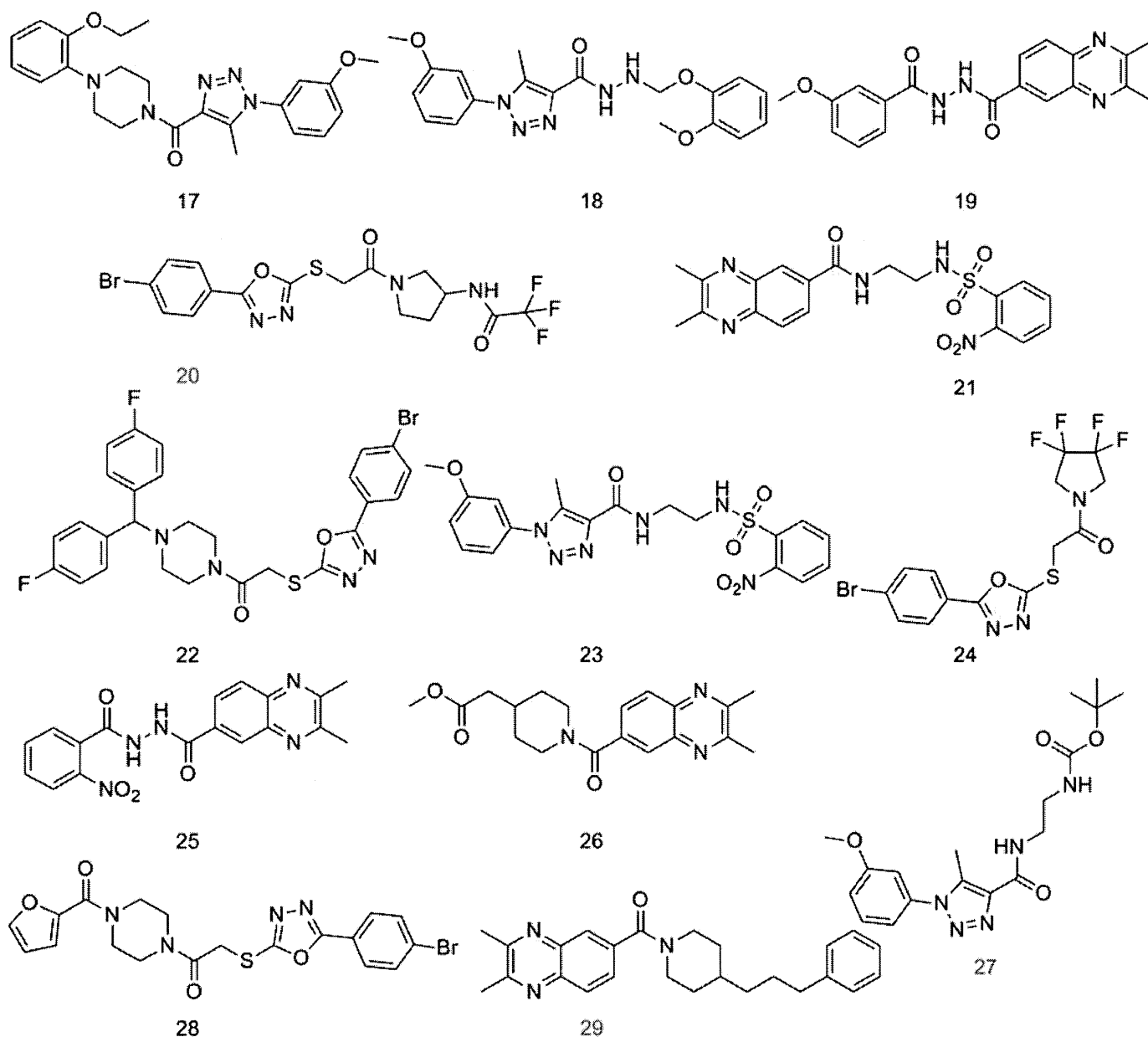
Fig. 4 (continued)

An active site covering the entire area of the two pockets in the CypA molecule was found using the SiteFinder module in MOE, and dummy atoms with hydrophobic or hydrophilic properties were placed into the two pockets to define the site.

Molecular docking

We docked AP back into the receptor (self-docking or re-docking) and screened the prepared database. For simplicity, flexibility of all of ligand atoms was allowed, in contrast to the receptor atoms during docking studies. We used five stages of the MOE Dock module to determine the potential docking poses of each ligand: (1) Dock was used to generate conformations from a single 3D conformer by applying a collection of preferred torsion angles to the rotatable bonds.

Here, a systematic search was conducted covering all combinations of angles on a grid if this resulted in fewer than 5,000 conformers. Otherwise, a stochastic sampling of conformations was conducted. (2) The collection of poses was generated from the pool of ligand conformations using the Triangle Matcher method, which can align ligand triplets of atoms on triplets of alpha spheres in a relatively systematic way. (3) Poses generated by the placement methodology were rescored using the London dG scoring function, and low scores were assigned to good poses. The top 30 poses were kept. (4) These 30 poses were refined using the explicit molecular mechanics forcefield method; at this time, the forcefield was set to MMFF94x. (5) Poses resulting from the refinement stage were rescored using the London dG scoring function. The top 30 poses of each compound were

retained for manual examination. Finally, candidates used for examination were selected according to the best docking score of each compound.

Inhibition of HIV-1 replication

Compounds were obtained from ChemGenesis, and positive control compounds were purchased from Namiki Shoji (http://www.namiki-s.co.jp/). Biological assays were performed to determine whether the compounds exert inhibitory effects on a single replication cycle of HIV-1. Briefly, 293T cells (1.5×10^6 cells in a 100-mm dish) were transfected with 8.9 μg of the pNL4-3-based [14], envelope glycoprotein-deficient HIV-1 proviral construct carrying a luciferase reporter gene, pNL-Luc-E$^-$R$^+$ [15], together with 1.1 μg of a vesicular stomatitis virus G protein (VSVG) expression plasmid, pHit/G [16], using FuGENE HD transfection reagent (Roche, Basel, Switzerland) to generate VSVG-pseudotyped HIV-1. Eighteen

Table 1 The screening results of 29 test compounds and two positive controls

Compound	Concentration [μM]	Inhibitory effect on HIV-1 replication[a]	Cytotoxicity[b]	Solubility[c]	Docking score[d]
1	40	−	−	−	−10.75
2	11	−	+	−	−10.69
3	30	−	+	−	−10.62
4	9	++	−	+	−10.61
5	12.5	−	+	−	−10.58
6	10	+	+	−	−10.58
7	40	−	−	−	−10.48
8	40	−	−	+	−10.41
9	40	−	+	+	−10.39
10	10	−	+	+	−10.35
11	40	−	+	−	−10.31
12	10	++	+	−	−10.29
13	6	−	+	−	−10.27
14	9	−	+	−	−10.26
15	10	−	+	+	−10.23
16	5	−	+	−	−10.22
17	10	−	+	−	−10.21
18	12.5	−	+	−	−10.20
19	40	−	+	−	−10.14
20	40	−	+	+	−10.11
21	40	−	+	−	−10.10
22	20	−	−	+	−10.10
23	9	++	+	−	−10.09
24	40	−	−	+	−10.09
25	40	−	−	−	−10.05
26	40	−	−	−	−10.03
27	40	−	+	−	−10.01
28	10	−	+	+	−10.00
29	10	−	+	−	−10.00
D4 [e]	40	++	−	−	NC[f]
FD8 [e]	40	++	−	−	NC[f]

[a] Viral replication was more than 30 % inhibited judging by the reduction of luciferase activity, which was not obviously due to the cytotoxicity of the compound, in both U87.CD4.CXCR4 and MT4 cell lines (++), in either cell line (+) or in neither cell line (−)

[b] The viability of 293T, U87.CD4.CXCR4, and/or MT4 cells was more (−) or less than 70 % (+) in the presence of the compound at 40 μM

[c] Presence (+) or absence (−) of crystals in DMEM medium containing 0.2 % DMSO

[d] The score was calculated by MOE

[e] Control compounds

[f] Not calculated

🖄 Springer

hours later, the transfected 293T cells were trypsinized and split into 200-μl subcultures in a 96-well plate in the presence of the indicated concentrations of a test compound. After 30 h of incubation, the cell culture supernatant was used to infect subconfluent U87.CD4.CXCR4 [17] or MT-4 cells treated with the corresponding compound. Twenty-four hours after infection, the luciferase activity in infected cells was measured using the Steady Glo Luciferase assay kit (Promega, Madison, WI) with a microplate luminometer (LB960, Berthold, Bad Wildbad, Germany) according to the manufacturer's protocol. The inhibitory effect of the compounds on viral replication was evaluated as the reduction in luciferase activity in infected cells. In addition, a cell toxicity test was performed using the WST-1 cell proliferation assay system (Roche) according to the manufacturer's protocol. Briefly, subconfluent 293T, U87.CD4.CXCR4, and MT-4 cells were treated with the indicated concentrations of a compound for 24 h. WST-1 reagent was then added to the cell culture, which was further

incubated until the absorbance of the samples at 450 nm was approximately 1.4 (approximately 1 h for 293T and U87.CD4.CXCR4 cells and 3 h for MT-4). The absorbance of the samples was measured using a microplate reader (Multiskan FC, Thermo Scientific, Rockford, IL), and the cytotoxicity of the compounds was evaluated as a reduction in absorbance. U87.CD4.CXCR4 cells were obtained through the AIDS Research and Reference Reagent Program (Division of AIDS, NIAID, NIH) from HongKui Deng and Dan R. Littman.

Structural analysis and residue interaction analysis

The interaction modes of the best poses of selected ligands were assessed using the Ligand Interactions module in MOE. The distances between important residues and ligands were measured. Subsequently, the best docking poses of active compounds in complex with
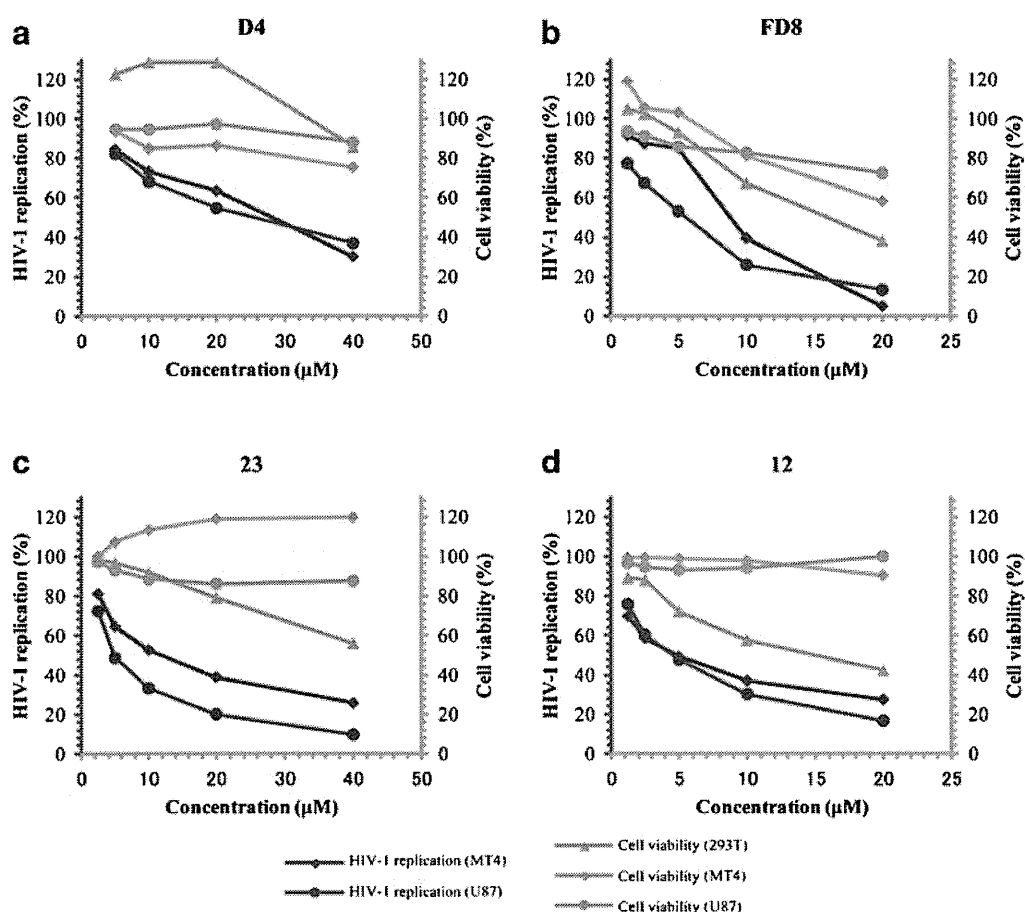

Fig. 5 Inhibitory effects on human immunodeficiency virus type 1 (HIV-1) replication and cellular toxicities of active compounds and controls. A vesicular stomatitis virus G protein-pseudotyped reporter virus was produced from 293T cells transfected with proviral DNA in the presence of various concentrations of the compound indicated. U87.CD4.CXCR4 or MT-4 cells were treated with a corresponding compound and then infected with the virus produced in the culture supernatant of 293T cells. Twenty-four hours after infection, the luciferase activity of infected cells was measured. The results are expressed

as a percentage of viral replication, which was calculated by determining the reduction in luciferase activity in the presence of a compound compared with that in the control experiment in the absence of the compound. All data points represent the means of two to four independent experiments. In addition, the cytotoxicity of each compound was measured using WST-1 reagent. The cytotoxicity of each compound is expressed as a percentage of the reduction in the absorbance in the presence of the compound

CypA were analyzed using IF-E 6.0 [18] (created by Dr. Hooman Shadnia at Carleton University), retrievable from the SVL exchange service. As mentioned in reports by Shadnia and others [18, 19], IF-E 6.0 can partition the native forcefield potentials and derive net interaction forces. It is used to decompose the interaction forces into three dimensions while analyzing the per-residue interactions. A list of positive and negative interaction energy values between a ligand and its neighbor receptor residues (within a defined distance range) can be calculated; negative values indicate favorable interactions, whereas positive values indicate unfavorable interactions. For our candidate ligands, receptor residues oriented less than 4.5 Å were analyzed.

Results and discussion

In silico screening

Comparison between X-ray crystal structure and structure determined by docking

To ensure the validity of our docking procedures and docking parameters before screening, we performed a test using the co-crystallographic data (pdb identifier: 2CYH) of CypA and AP (Fig. 1) [12]. AP was isolated from the complex and then re-docked into the receptor CypA using the MOE software package. The best docking pose to emerge from our docking differed from the original conformation only by 0.261 Å in root mean square deviation (RSMD). Therefore, we selected the pose displaying the lowest docking score as the best pose. Figure 2 shows the comparison between the X-ray crystal structure (colored in red) of AP and the best docking pose (colored in blue).

Basic properties of compounds in the target database

We selected a commercially available database from ChemGenesis (http://www.all-chemy.com/) containing 1,377 low-molecular-weight compounds as the source database. The drug-likeness of these compounds was calculated by the QuaSAR-Descriptor module in MOE. More than 85 % of the compounds obeyed drug-likeness (the number of violations of Lipinski's Rule of Five [13] was less than two). Although less drug-like compounds are usually removed from the target database before docking, because of the small number of compounds in the database, both drug-like and less drug-like compounds were tested. The calculated molecular weights of compounds varied between 201.2 and 622.8 Da, and 1,325 compounds had molecular weights of less than 500 Da. According to the pocket size of

CypA, the diameters of the compounds, which varied between 7 and 30 Å, were considered suitable, and no compounds were rejected before performing docking studies.

Analysis of receptor properties and definition of docking sites

According to the co-crystal data of CypA/AP, CypA adopts an eight-stranded antiparallel beta barrel structure (Fig. 1a), and AP is buried deeply in one of the cavities on the surface of CypA (Fig. 1b). This cavity is also where CsA, the HIV CA fragment, and other substrates bind. The most important residues of this cavity were identified by site-directed mutagenesis (Arg55, Phe60, Phe113, and His126) [20]. This cavity has also been called Site A or the MVA11-binding pocket (according to CsA binding mode) in previous reports [8, 21]. Over a saddle-like region, there is another hydrophobic pocket called Site B, or the Abu2-binding pocket. In addition to Sites A and B, there is also some empty space above, referred to here as Site C (Fig. 1b). Although the co-crystallographic data of the CypA/CA fragment indicate that Site A should be the direct docking site, Sites B or C could be considered an auxiliary cavity when compounds possess important elongated functional groups. Therefore, using the SiteFinder module in MOE, we defined a larger docking region contained among Sites A, B and C, and docked compounds in the target database into CypA.
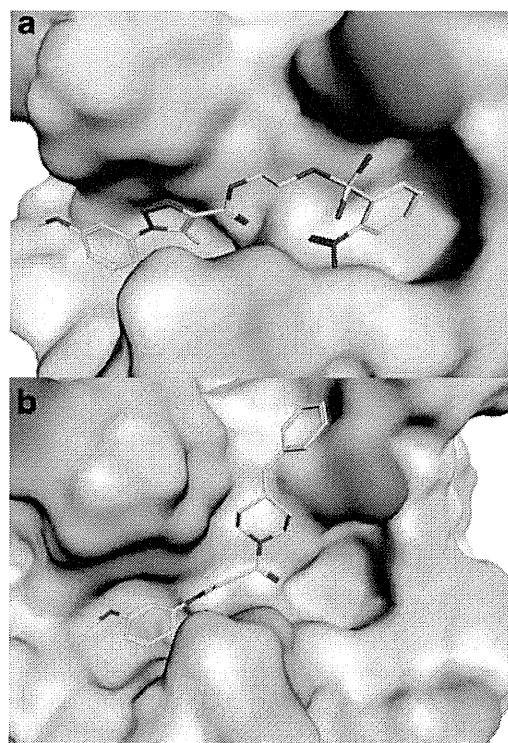

Fig. 6a,b Docking poses of two active compounds: **23** and **12**. **23** binds using Mode 1 (**a**), and **12** binds using Mode 2 (**b**)

Selection of compounds for biological evaluation

According to the predicted fitting score, which expresses the lowest binding energy of a certain pose, we selected 29 compounds, as shown in Figs. 3, and two previously reported active compounds as controls [8, 22]. We observed two binding modes: (1) molecules covering both Site A and Site B; and (2) molecules placed into Site B and Site C, but not Site A (Fig. 4). Of the 29 compounds listed in Fig. 3, 20 bound in the style of Mode 1 (Fig. 4a), and 9 compounds in the style of Mode 2 (Fig. 4b), as the lowest scored poses.

Site A was confirmed to be responsible for the PPIase activity of CypA and to serve as the binding site of the CA fragment of HIV and CsA, and thus several groups have made efforts to locate compounds that can fill this pocket as much as possible by screening and/or molecular design experiments [8, 21, 22]. Therefore, molecules that interact with CypA in Mode 1 were more likely to be investigated; however, the inhibitory activities of most of the candidates were limited to the micromolar level. To find potent inhibitor candidates with novel skeletons, we kept both Mode 1 and Mode 2 compounds for further biological evaluation.

Experimental results of viral replication and cell viability

Biological assays were performed to determine whether the 29 compounds and the 2 positive controls exerted inhibitory effects on viral replication and induced cellular toxicity. 293T cells were employed as virus-producing cells, whereas a T cell line, MT-4, and a reporter cell line expressing HIV-1 receptors, U87.CD4.CXCR4, were used as viral target cells. This assay system can evaluate the inhibitory effects of test compounds in a single replication cycle of HIV-1. The results demonstrated that most of the other tested compounds either did not exert noticeable inhibitory effects on HIV-1 replication or exhibited strong cytotoxicity at higher concentrations (Table 1). Moreover, although compound 4 exerted an inhibitory effect on viral replication, it displayed low solubility (Table 1); therefore, we did not evaluate this compound further. By contrast, two of our compounds, 12 and 23, as well as the two positive control compounds, exerted potent inhibitory effects on HIV-1 replication while exhibiting low cytotoxicity at the effective concentration inhibiting viral growth by 50 % (Fig. 5). Compared with the control compounds D4 and FD8, our hit compounds exhibited stronger inhibitory activities.
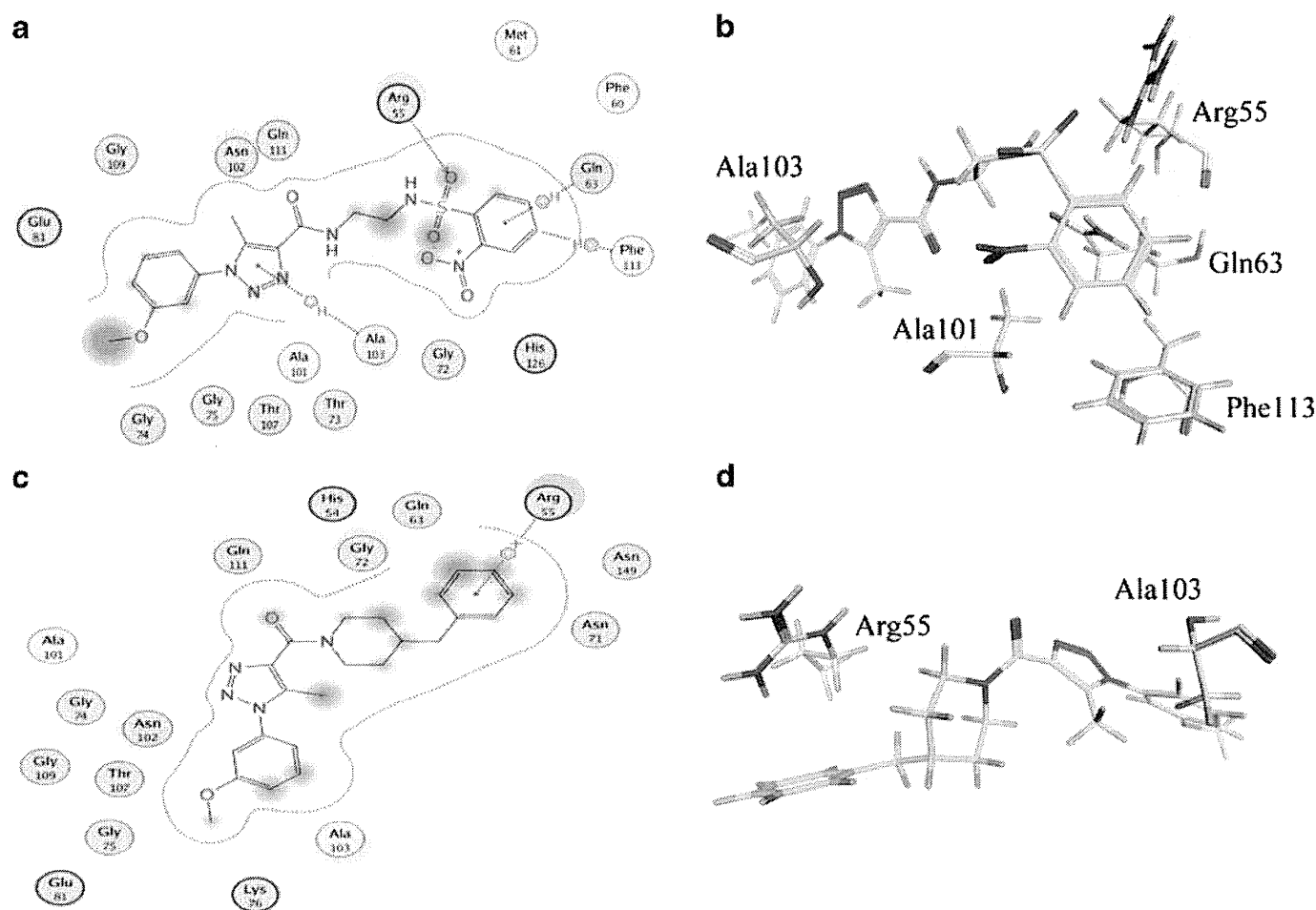

Fig. 7 Schematic view and docking pose of compound **23** (**a**, **b**) and compound **12** (**c**, **d**) with their binding sites. For docking poses, only important residues are displayed
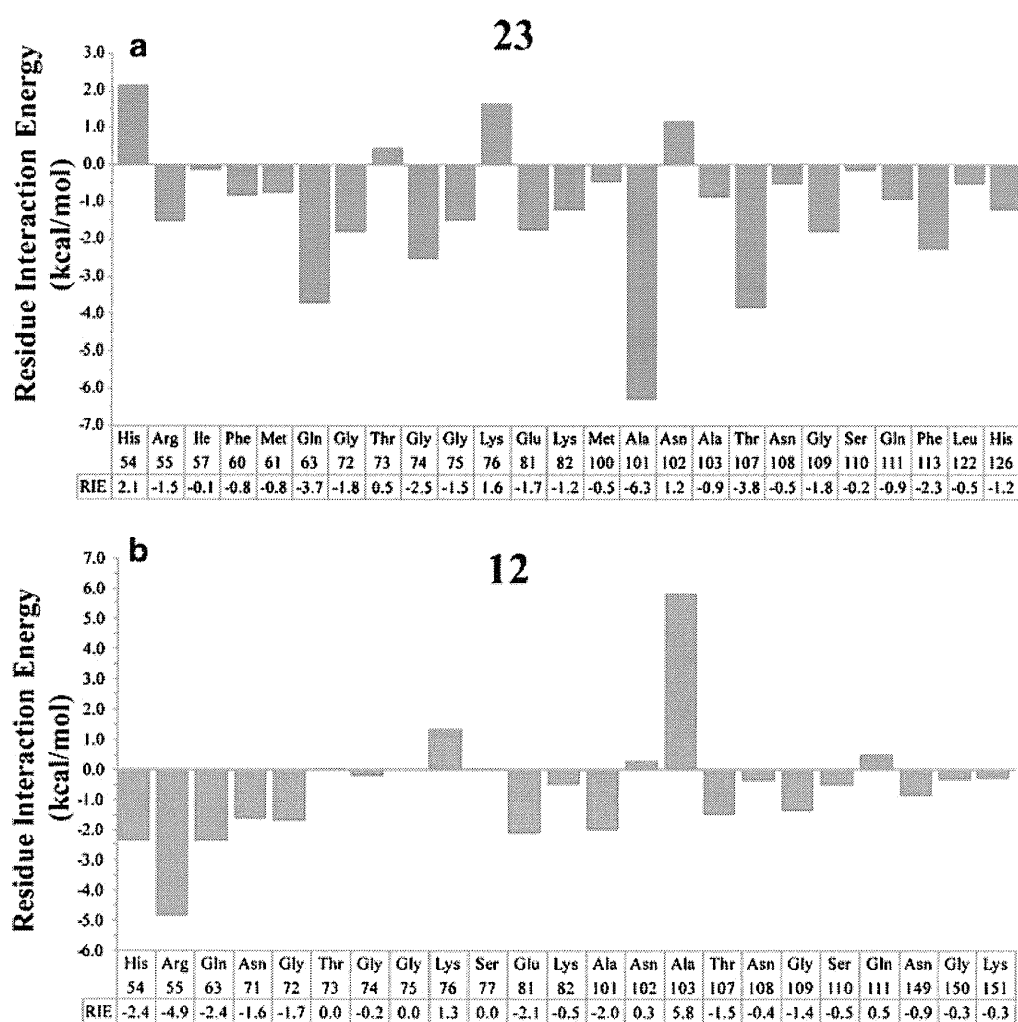
Structural analysis of active compounds

The docking poses of compounds **23** and **12** were different. The best docking pose of **23** utilized Mode 1 binding (Fig. 6a), whereas that of **12** utilized Mode 2 binding (Fig. 6b). The interactions were first assessed using the Ligand Interactions module in MOE. These analyses provided direct schematic views of the interactions of **23** and **12** with CypA, as shown in Fig. 7a and c, respectively. Compound **23** inserted into both Site A and Site B. Figure 7a and b illustrate the dimensional interaction maps and docking poses, respectively, of **23** with CypA. The presence of 2-nitrobenzenesulfonamide appears responsible for the binding between **23** and Site A of CypA. The oxygen atom in the sulfonamide group interacts with the nitrogen atom at the ω position of Arg55 (**23**: O – CypA: Arg55: N^{ω}) within a distance of 2.9 Å. The aromatic ring of nitrobenzene interacts with both Gln63 and Phe113. Two edge-to-end (T-shaped) hydrogen-aromatic ring interactions (**23**:aromatic ring–CypA:Gln63:H and **23**:aromatic hydrogen–CypA:Phe113:aromatic ring) form a π–π stacking network. Because Arg55 and Phe113 are important pocket-forming residues and are highly conserved in most CypA

isolates, these interactions are very meaningful for inhibitor design. Another key interaction revealed in the interaction map is the hydrophobic interaction between Ala103 and the triazole group of **23**. For **12**, arene-cation interactions (**12**: benzene ring–CypA: Arg55: NH1 and NH2) were detected. As mentioned above, Arg55 is a critical residue for ligand binding. These interactions can partly explain the activity of **12**.

Geometry-based interaction fingerprints provided loosely approximated insights into the fitting of our two active compounds into the receptor sites. However, it is difficult to determine the detailed intermolecular energies, particularly in terms of hydrophobic interactions. Therefore, we performed additional post-docking analyses. The interactions between binding site residues and active compounds were scrutinized using IF-E 6.0 [18] (created by Dr. Hooman Shadnia at Carleton University, http://www.shadnia.com/H_IFE/index.htm), retrievable from the SVL exchange service. This program can differentiate favorable ligand–residue interactions from unfavorable ones by force vectors and energy values. A negative sign indicates a stable interaction, whereas a positive sign indicates an unstable or repulsive interaction. The results of **23** and **12** for each residue near ligand atoms (less than 4.5 Å in distance) are

Fig. 8a,b Ligand–receptor interaction energy values (per-residue values) calculated using IF-E 6.0. The residue interaction energy data values are expressed in kcal mol^{-1}. **a** Graph for **23**, **b** graph for **12**

	His 54	Arg 55	Ile 57	Phe 60	Met 61	Gln 63	Gly 72	Thr 73	Gly 74	Gly 75	Lys 76	Glu 81	Lys 82	Met 100	Ala 101	Asn 102	Ala 103	Thr 107	Asn 108	Gly 109	Ser 110	Gln 111	Phe 113	Leu 122	His 126
RIE	2.1	-1.5	-0.1	-0.8	-0.8	-3.7	-1.8	0.5	-2.5	-1.5	1.6	-1.7	-1.2	-0.5	-6.3	1.2	-0.9	-3.8	-0.5	-1.8	-0.2	-0.9	-2.3	-0.5	-1.2

	His 54	Arg 55	Gln 63	Asn 71	Gly 72	Thr 73	Gly 74	Gly 75	Lys 76	Ser 77	Glu 81	Lys 82	Ala 101	Asn 102	Ala 103	Thr 107	Asn 108	Gly 109	Ser 110	Gln 111	Asn 149	Gly 150	Lys 151
RIE	-2.4	-4.9	-2.4	-1.6	-1.7	0.0	-0.2	0.0	1.3	0.0	-2.1	-0.5	-2.0	0.3	5.8	-1.5	-0.4	-1.4	-0.5	0.5	-0.9	-0.3	-0.3

presented in Fig. 8. For **23**, in addition to the important residues mentioned above, we can see that Ala101 is also responsible for binding (Fig. 8a). The carbon in the Ala101 backbone is in approximation with the carbonyl oxygen of **23** (separated by 3.57 Å) (Fig. 7a). The dispersion force between the electron-poor environment of the Ala101 backbone carbon and the electron-rich environment of the carbonyl oxygen of **23** resulted in good binding effects. For **12**, the negative-signed interaction energy values, which indicate favorable residues for ligand binding, could be detected at multiple residues of CypA including the aforementioned residue Arg55. In addition to Arg55, other favorable residues for binding are listed in Fig. 8b. Conversely, a strong signal for a positive-signed peak could be detected at Ala103, suggesting that it is an unfavorable residue for the binding of **12**. By assessing atomic distances, we found that the methyl hydrogen atom of the Ala103 side chain and the aromatic hydrogen atom of **12** are approximately 1.8 Å apart (Fig. 7d). It can be concluded that the two hydrogen atoms clash with each other. However, it should be underlined that this docking pose was obtained from a rigid receptor docking procedure; therefore, this model cannot explain any "induced-fitting" phenomena. We assume that, due to the strong repulsion detected, the receptor residue should shift into a more appropriate orientation in a real system.

Compounds **23** and **12** have similar skeletons; however, they exhibited different docking modes. Molecules that target the combination region of the two modes can be assumed to be more active. These types of combined molecules are now under investigation using in-silico-based methods.

Conclusions

The present work involved the discovery of HIV-1 inhibitors targeting CypA via in silico and biological screening methods. Twenty-nine compounds selected from a database, together with control compounds, were examined for antiviral activities. Two of the compounds exhibited comparatively good effects in biological assays. In particular, compounds **12** and **23** both exhibited anti-HIV-1 activities with relatively low cytotoxicity at the effective concentration inhibiting viral growth by 50 %. From our experimental results, **12** and **23** may be used as lead compounds for novel type of anti-HIV inhibitors, although biochemical experiments to confirm that the target is really CypA are still needed.

References

1. Ke H, Huai Q (2003) Structures of calcineurin and its complexes with immunophilins-immunosuppressants. Biochem Biophys Res Commun 311:1095–1102
2. Foster TL, Gallay P, Stonehouse NJ, Harris M (2011) Cyclophilin A interacts with domain II of hepatitis C virus NS5A and stimulates RNA binding in an isomerase-dependent manner. J Virol 85:7460–7464
3. Chatterji U, Bobardt MD, Lim P, Gallay PA (2010) Cyclophilin A-independent recruitment of NS5A and NS5B into hepatitis C virus replication complexes. J Gen Virol 91:1189–1193
4. Chen Z, Mi L, Xu J, Yu J, Wang X, Jiang J, Xing J, Shang P, Qian A, Li Y, Shaw PX, Wang J, Duan S, Ding J, Fan C, Zhang Y, Yang Y, Yu X, Feng Q, Li B, Yao X, Zhang Z, Li L, Xue X, Zhu P (2005) Function of HAb18G/CD147 in invasion of host cells by severe acute respiratory syndrome coronavirus. J Infect Dis 191:755–760
5. Lin TY, Emerman M (2006) Cyclophilin A interacts with diverse lentiviral capsids. Retrovirology 3:70
6. Zenke G, Strittmatter U, Fuchs S, Quesniaux VF, Brinkmann V, Schuler W, Zurini M, Enz A, Billich A, Sanglier JJ, Fehr T (2001) Sanglifehrin A, a novel cyclophilin-binding compound showing immunosuppressive activity with a new mechanism of action. J Immunol 166:7165–7171
7. Li Q, Moutiez M, Charbonnier JB, Vaudry K, Menez A, Quemeneur E, Dugave C (2000) Design of a Gag pentapeptide analogue that binds human cyclophilin A more efficiently than the entire capsid protein: new insights for the development of novel anti-HIV-1 drugs. J Med Chem 43:1770–1779
8. Li J, Tan Z, Tang S, Hewlett I, Pang R, He M, He S, Tian B, Chen K, Yang M (2009) Discovery of dual inhibitors targeting both HIV-1 capsid and human cyclophilin A to inhibit the assembly and uncoating of the viral capsid. Bioorg Med Chem 17:3177–3188
9. Chen K, Tan Z, He M, Li J, Tang S, Hewlett I, Yu F, Jin Y, Yang M (2010) Structure-activity relationships (SAR) research of thiourea derivatives as dual inhibitors targeting both HIV-1 capsid and human cyclophilin A. Chem Biol Drug Des 76:25–33
10. Vajdos FF, Yoo S, Houseweart M, Sundquist WI, Hill CP (1997) Crystal structure of cyclophilin A complexed with a binding site peptide from the HIV-1 capsid protein. Protein Sci 6:2297–2307
11. Mikol V, Kallen J, Pflugl G, Walkinshaw MD (1993) X-ray structure of a monomeric cyclophilin A-cyclosporin A crystal complex at 2.1 A resolution. J Mol Biol 234:1119–1130
12. Zhao Y, Ke H (1996) Mechanistic implication of crystal structures of the cyclophilin-dipeptide complexes. Biochemistry 35:7362–7368
13. Lipinski CA, Lombardo F, Dominy BW, Feeney PJ (1997) Experimental and computational approaches to estimate solubility and permeability in drug discovery and development settings. Adv Drug Deliv Rev 23:3–25
14. Adachi A, Gendelman HE, Koenig S, Folks T, Willey R, Rabson A, Martin MA (1986) Production of acquired immunodeficiency syndrome-associated retrovirus in human and nonhuman cells transfected with an infectious molecular clone. J Virol 59:284–291
15. Tokunaga K, Greenberg ML, Morse MA, Cunning RI, Lyerly HK, Cullen BR (2001) Molecular basis for cell tropism of CXCR4-dependent human immunodeficiency virus type 1 isolates. J Virol 75:6776–6785
16. Fouchier RA, Meyer BE, Simon JH, Fischer U, Malim MH (1997) HIV-1 infection of non-dividing cells: evidence that the amino-terminal basic region of the viral matrix protein is important for Gag processing but not for post-entry nuclear import. EMBO J 16:4531–4539
17. Björndal A, Deng H, Jansson M, Fiore JR, Colognesi C, Karlsson A, Albert J, Scarlatti G, Littman DR, Fenyö EM (1997) Coreceptor

usage of primary human immunodeficiency virus type 1 isolates varies according to biological phenotype. J Virol 71:7478–7487

18. Shadnia H, Wright JS, Anderson JM (2009) Interaction force diagrams: new insight into ligand-receptor binding. J Comput Aided Mol Des 23:185–194

19. Dal Ben D, Buccioni M, Lambertucci C, Marucci G, Thomas A, Volpini R, Cristalli G (2010) Molecular modeling study on potent and selective adenosine A(3) receptor agonists. Bioorg Med Chem 18:7923–7930

20. Zydowsky LD, Etzkorn FA, Chang HY, Ferguson SB, Stolz LA, Ho SI, Walsh CT (1992) Active site mutants of human cyclophilin

A separate peptidyl-prolyl isomerase activity from cyclosporin A binding and calcineurin inhibition. Protein Sci 1:1092–1099

21. Guichou JF, Viaud J, Mettling C, Subra G, Lin YL, Chavanieu A (2006) Structure-based design, synthesis, and biological evaluation of novel inhibitors of human cyclophilin A. J Med Chem 49:900–910

22. Chen S, Zhao X, Tan J, Lu H, Qi Z, Huang Q, Zeng X, Zhang M, Jiang S, Jiang H, Yu L (2007) Structure-based identification of small molecule compounds targeting cell cyclophilin A with anti-HIV-1 activity. Eur J Pharmacol 565:54–59

Original Paper

Intervirology

Chikungunya Virus Induces a More Moderate Cytopathic Effect in Mosquito Cells than in Mammalian Cells

Yong-Gang Li[a]   Uamporn Siripanyaphinyo[b]   Uranan Tumkosit[b]
Nitchakarn Noranate[b]   Atchareeya A-nuegoonpipat[c]   Ran Tao[a]   Kurosu Takeshi[a]
Kazuyoshi Ikuta[a]   Naokazu Takeda[b]   Surapee Anantapreecha[c]

[a]Department of Virology, Research Institute for Microbial Diseases, Osaka University, Osaka, Japan; [b]Section of Viral Infections, Thailand-Japan Research Collaboration Center on Emerging and Re-Emerging Infections, and [c]National Institute of Health, Department of Medical Sciences, Ministry of Public Health, Nonthaburi, Thailand

Abstract
Objectives: Chikungunya virus (CHIKV) is an alphavirus belonging to the Togaviridae family. Alphaviruses cause a chronic non-cytopathic infection in mosquito cells, while they develop a highly cytopathic infection in cells originating from various vertebrates. In this study, we compared the cytopathic effect (CPE) induced by CHIKV in Vero cells and a mosquito cell line, C6/36 cells. *Methods:* CPE and the virus titers were compared between the CHIKV-infected C6/36 and Vero cells. Apoptosis was measured by TUNEL assay, and the differences between the C6/36 and Vero cells were compared. *Results:* CHIKV infection induced strong CPE and apoptosis in the Vero cells, but light CPE in the C6/36 cells. The virus titers produced in the C6/36 cells were much higher than those produced in the Vero cells. *Conclusions:* The reason CHIKV induced strong CPE is that this virus triggers strong apoptosis in Vero cells compared with C6/36 cells. CHIKV established a persistent infection in C6/36 cells after being passaged 20 times. CHIKV infection in mosquito cells was distinct from that in Vero cells. The cell and species specificity of CHIKV-induced cell death implies that the cellular and viral regulators involved in apoptosis may play an important role in determining the outcome of CHIKV infection.

Copyright © 2012 S. Karger AG, Basel

Introduction

Chikungunya virus (CHIKV), the causative agent of chikungunya fever, was first described in 1952 during an epidemic in Tanzania, East Africa [1]. CHIKV is a positive-sense single-strand RNA virus belonging to the genus *Alphavirus* in the family Togaviridae, and is maintained in two distinct transmission cycles, a sylvatic cycle and human-mosquito-human cycle. The scale of the epidemics for the former is smaller than the latter, and mainly confined within African countries involving primates, such as monkeys and forest-dwelling Aedes mosquitoes [2, 3]. The main vectors of CHIKV transmission in the human-mosquito-human cycle are *Aedes aegypti and Aedes albopictus*. Since its first outbreak in East Africa,

Yong-Gang Li
Department of Virology
Research Institute for Microbial Diseases
Osaka University, Osaka (Japan)
Tel. +81 6 6879 8309, E-Mail yonggang@biken.osaka-u.ac.jp

CHIKV epidemics have often been characterized by long interepidemic periods of more than 10 years in many parts of Southern and Southeast Asia [4, 5]. During the past 8 years, the major outbreaks have occurred on islands in the Indian Ocean. Reunion Island has been among the most severely hit, with one third of its population infected and more than 240 deaths recorded [6]. The symptoms of chikungunya generally start 4–7 days after the bite, and the acute phase, lasting 1–10 days, is characterized by painful polyarthralgia, high fever, asthenia, headache, vomiting, rash, and myalgia [1, 7]. Chikungunya has affected as many as 3–4 million people in the Indian Ocean zone; it spread to Europe in 2005–2007, and recent outbreaks in Thailand have received considerable attention [8].

Both mosquito and vertebrate cell culture systems have been used to study CHIKV replication and pathogenesis [9]. Mosquito cells derived originally from *A. albopictus* larvae in particular have been employed in these studies. CHIKV is also able to infect a wide range of vertebrate cells and cell lines [10, 11], and most of these show an apparent cytopathic effect (CPE) [9]. A similar phenomenon was found in sindbis virus (SINV) infection, where almost all vertebrate cells died after infection, and the cell lines derived from mosquito are known to provide a long-term persistent infection [12]. The cell line derived from mosquito is known to provide a long-term persistent infection which is probably maintained by intracellular factors [13]. The viruses belonging to the alphavirus family have appeared to grow in cultured vertebrate and invertebrate cells [14]. Although alphaviruses cause encephalitis, neuronal apoptosis and death in mammals, they fail to kill the mosquitoes that can transmit these viruses. Therefore, host cell factors as well as viral factors regulate the outcome of the infection [15].

SINV is thought to cause a persistent infection in mosquito cells with moderate CPE in general [16]. We thought that CHIKV might also cause milder CPE in mosquito cells than in mammalian cells, and would lead to persistent infection in mosquito cells. The study on the pathogenicity of CHIKV is inadequate. Since Vero cells and C6/36 cells are commonly used in the propagation of flaviviruses such as dengue virus and togaviruses such as SINV [17–19], we used these two cells to study the pathogenesis of CHIKV infection. We found that CHIKV induced light CPE in mosquito cells, C6/36, but strong CPE in Vero cells. C6/36 produced higher titers of the progeny viruses compared to the Vero cells. CHIKV seems to establish a persistent infection in C6/36 cells when passaged

20 times. Interestingly, we also found that CHIKV induced stronger apoptosis in Vero cells than in C6/36 cells, although the mechanism is not yet known.

Materials and Methods

Virus and Cells
CHIKV Ross strain was propagated in Vero-E6 (Vero) cells which were maintained in MEM supplemented with 10% newborn calf serum and antibiotics at 37° in 5% CO_2. C6/36 cells were maintained in Leibovitz's L-15 Media (Invitrogen, Carlsbad, Calif., USA) supplemented with 10% newborn calf serum, antibiotics and 1% TPB (Sigma, St. Louis, Mo., USA) at 32°. All experiments were performed in a biosafety level 3 containment laboratory.

Immunofluorescence Assay
CHIKV- and mock-infected cells were fixed with 4% paraformaldehyde, and incubated 30 min at 37° with monoclonal antibody against the CHIKV E2 protein followed by FITC-conjugated anti-mouse IgG (Invitrogen) for 30 min at 37°. The monoclonal antibody was provided by Dr. P. Depres [20].

Plaque Assay
Vero cells were seeded at 1×10^6 cells per well in 6-well plates and incubated at 37° overnight. The cells were washed once with phosphate-buffered saline (PBS). Ten-fold serial dilutions of the virus were prepared in Hanks Buffer (Sigma-Aldrich), and 0.2 ml of the solution was inoculated into each well and incubated for 1 h at 37°. During incubation, the plates were gently agitated every 15 min. After the adsorption, the virus solution was removed and the cells washed three times with PBS. Two ml of 1% agrose in $2\times$ MEM containing 0.5% FBS was layered onto the cell monolayers. The plates were incubated in a humidified incubator at 37° with 5% CO_2 for 3 days, and then the agarose overlay was removed and washed with PBS. The plaques were visualized by staining the monolayer with 2 ml of 0.25% crystal violet in 10% formaldehyde solution (Sigma-Aldrich) for 2 h at room temperature. The plates were washed and the plaques counted.

TUNEL Staining
The Vero and C6/36 cells (2×10^6) were infected at a multiplicity of infection (MOI) 1, and apoptotic cells were characterized by terminal deoxynucleotidyl transferase-mediated dUTP-biotin nick end labeling according to the manufacturer's instructions (DeadEnd Fluorometric TUNEL System; Promega). Briefly, after 24-hour postinfection (p.i.), the cells were fixed with 3% of paraformaldehyde in PBS containing 0.1% Triton X-100, washed with PBS three times, and incubated in a labeling reaction mixture containing terminal deoxynucleotidyl transferase enzyme, fluorescein isothiocyanate-conjugated nucleotide, and labeling buffer. The reaction was quenched in stop buffer, and the cells were washed with PBS several times. The cell nuclei were counterstained with propidium iodide (Sigma-Aldrich). Apoptosis was induced by a protein synthesis inhibitor, anisomycin, according to the manufacturer's instructions, and used as the positive control.
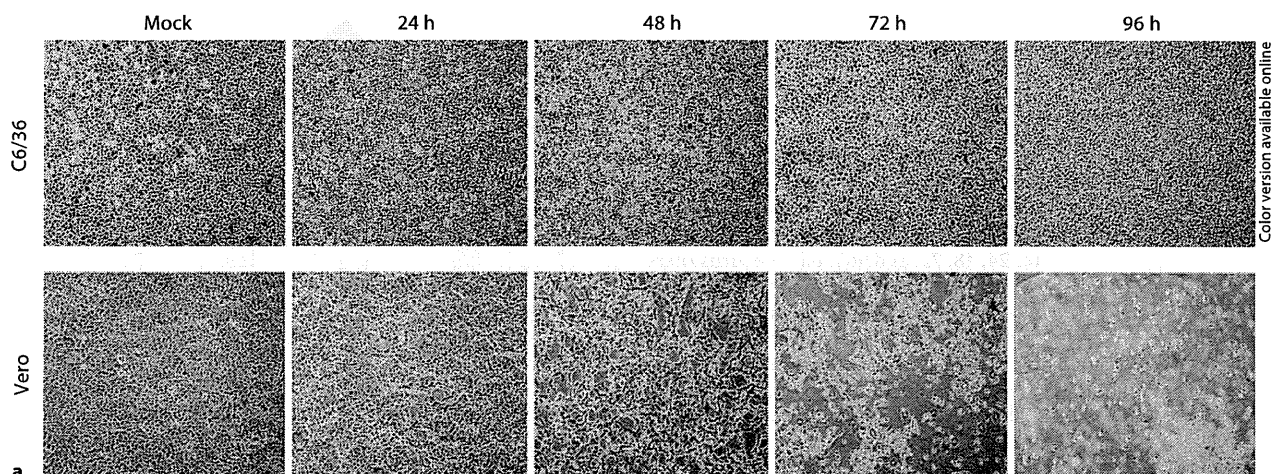
Li et al.

Fig. 1. a CPE of C6/36 and Vero cells infected with CHIKV. C6/36 and Vero cells were seeded in 12-well plates, infected with CHIKV at MOI 1 and incubated at 32°. CPE was observed under a microscope at 24, 48, 72 and 96 h p.i. Mock infection was shown at 96 h p.i. The morphology of the infected cells was photographed. ×400. **b** Immunofluorescence staining of CHIKV-infected C6/36 cells. The cells were incubated with a monoclonal antibody against CHIKV E2 protein and labeled with FITC at 24, 48 and 72 h p.i. ×400.
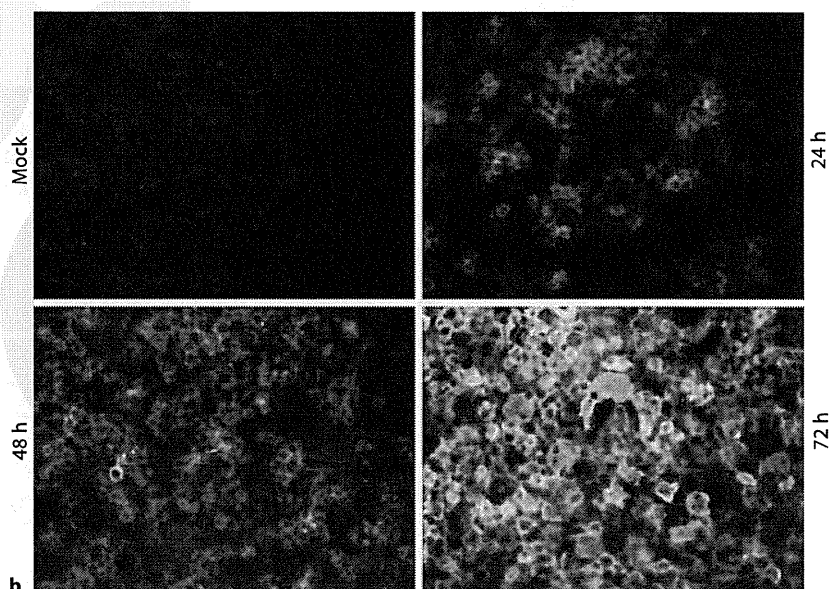
Results

CHIKV Induced Moderate CPEs in C6/36 and Strong CPEs in Vero Cells

Vero cells and C6/36 cells were infected with CHIKV at MOI 1. After 24, 48, 72, and 96 h p.i., the CPE was observed directly under a light microscope. In the primary experiment, we performed the experiment under different temperatures at 28, 32, and 37°. No effect was observed at 32°on the viability of Vero cells after 48 h (data not shown), and both Vero and C6/36 cells were incubated at 32°to avoid the effectiveness of the temperature.

The Vero cells showed apparent CPE at 48 h p.i., and nearly 90% of the cells died at 96 h p.i. In contrast, C6/36 showed minute CPE at 96 h p.i. (fig. 1a). To examine the expression of the viral E2 protein in C6/36 cells, an immunofluorescence assay was carried out at 24, 48, and 72 h p.i. The C6/36 cells were nearly 80% positive at 48 h p.i., and 100% at 72 h p.i. (fig. 1b). The Vero cells were 80% positive at 24 h p.i. (data not shown). These results indicated that the C6/36 cells showed moderate CPE under the condition in which the virus replication occurred in all of the infected cells.

Fig. 2. Virus titers in the supernatant of CHIKV-infected C6/36 and Vero cells. C6/36 and Vero cells were infected with CHIKV at MOI 1 and incubated at 32°. After 24, 48, 72, and 96 h p.i., the virus titers in the medium were determined by a plaque assay. The mean titers from three replicates are shown with the standard deviations. Statistical significance between the virus titers from the C6/36 and Vero cells at different time points (p < 0.01) are marked with an asterisk.
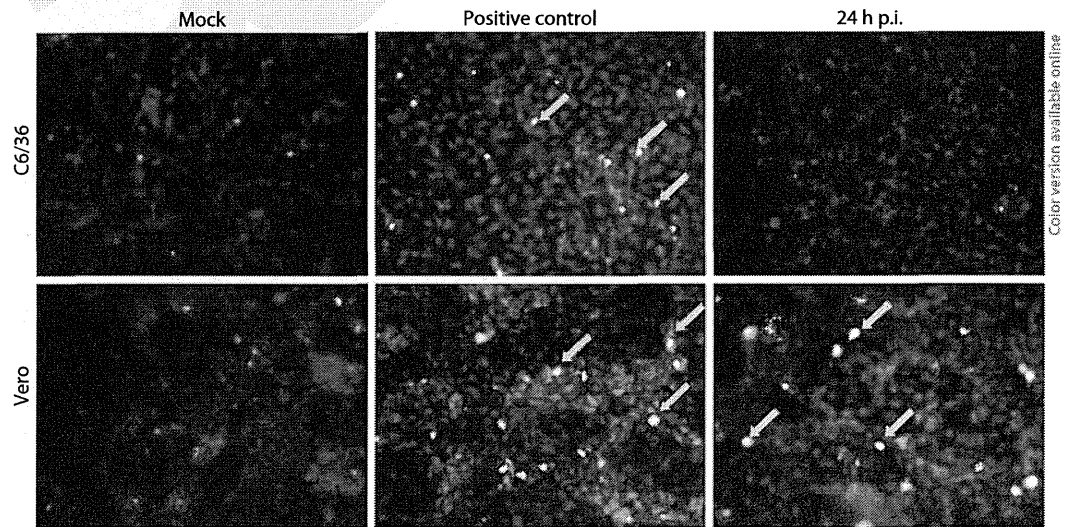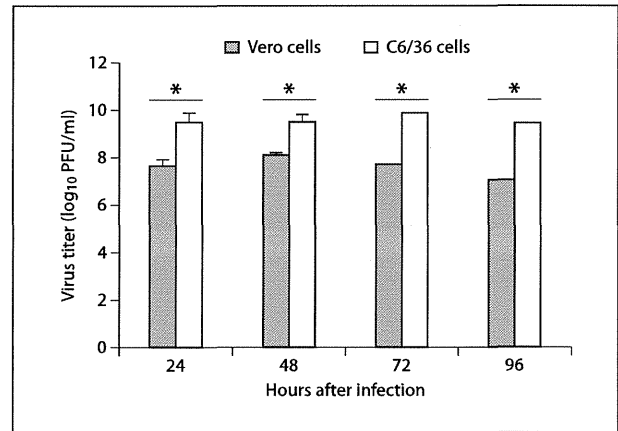

Fig. 3. TUNEL assay with CHIKV-infected C6/36 and Vero cells at 24 h p.i. at 32°. Cells with the arrows indicate apoptotic cells (green). Propidium iodide was used to stain the nuclei (red). The positive controls were cells treated with a protein synthesis inhibitor, anisomycin.

Virus Titers in Infected Vero and C6/36 Cells

The Vero and C6/36 cells were infected with CHIKV at MOI 1, and the virus titers in the culture medium were measured by a plaque assay as described in 'Materials and Methods'. The mean virus titers produced in the C6/36 cells were 8.5×10^9, 1.8×10^{10}, 1.7×10^{10} and 3×10^9 PFU/ml at 24, 48, 72 and 96 h p.i., whereas those in the Vero cells were 9×10^7, 1×10^8, 7×10^7, and 1.5×10^7 PFU/ml (fig. 2), indicating that the C6/36 cells produced higher viral titers than the Vero cells. The C6/36 cells produced a viral titer that was more than 100 times higher than the Vero cells. More than 100 times viruses were produced in the C6/36 cells. Although the Vero cells showed strong CPE, the levels of virus replication were not efficient. These results coincided with those in a previous report obtained from SINV, in which CPE did not affect the virus titer that much [21].
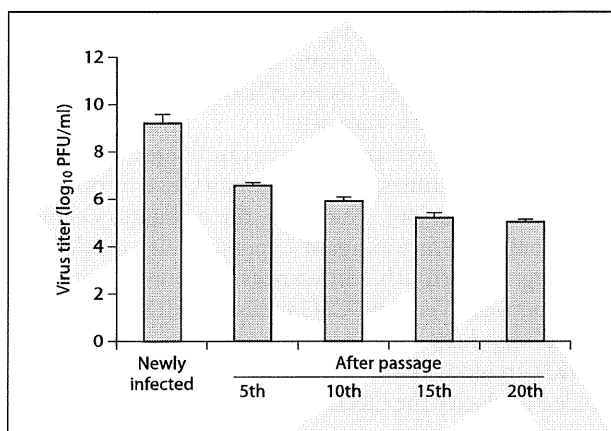
Fig. 4. Virus titers in the supernatant from CHIKV-infected C6/36 cells measured by a plaque assay. C6/36 cells were newly seeded every 3 days, and passaged 20 times at 32°.

Apoptosis of Vero and C6/36 Cells after Infection with CHIKV

In order to explore the mechanism of CHIKV-induced CPE in Vero cells, we analyzed apoptosis. Following infection or mock infection, the cells were fixed and subjected to TUNEL analysis as described in 'Materials and Methods'. As depicted in figure 3, the Vero cells at 24 h p.i. showed several apoptotic cells (green), but very few apoptotic cells were found in the CHIKV-infected C6/36 cells, suggesting that apoptosis may be one of the reasons why strong CPE was induced in the Vero cells.

CHIKV Caused Persistent Infection in C6/36 Cells

To examine whether CHIKV causes persistent infection in the mosquito cells, C6/36 cells were infected with CHIKV at MOI 1, incubated for 5 days at 32°, and then passaged 20 times every 3 days using 1×10^6 cells for each passage. The medium was collected on day 3 in every passage, and the virus titers were determined and compared. The virus titers were 4.5×10^6, 1.25×10^6, 2.5×10^5 and 1.5×10^5 in the 5th, 10th, 15th, and 20th passages, respectively, showing a decreasing trend, although the titers were not significantly different between each passage (fig. 4). After 20 passages, the expression of the viral antigen was examined by immunofluorescence assay, and nearly 100% of the cells were infected (data not shown). These results indicated that CHIKV had established a persistent infection in the C6/36 cells.

Discussion

Alphaviruses are generally thought to cause a lytic infection (apoptosis) in many mammalian cells, while they cause a persistent infection in mosquito cells exhibiting moderate CPE. For example, SINV causes acute cell death in most types of mammalian cells, and the infected cells display typical characteristics of apoptosis [21]. SINV is generally thought to cause only moderate CPE in mosquito cells with a persistent infection [16]. Similarly, dengue virus, a member of the flavivirus family, does not cause deleterious effects in mosquito cells and may result in persistent infection [22], suggesting that the cellular response to some of the members of the alphavirus and flavivirus families is highly related to the cell type. The reasons why SINV infection does not cause apoptosis in mosquito cells are still obscure.

CHIKV is a member of the alphavirus family, and causes a re-emerging mosquito-borne infection. In this study, we observed the same phenomenon in CHIKV as in SINV, in which CHIKV induced strong CPE and apoptosis in Vero cells, but light CPE and apoptosis in C6/36 mosquito cells. Apoptosis in HeLa cells induced by CHIKV was recently characterized, and this virus was found to trigger apoptosis through an early caspase-9-dependent intrinsic mitochondrial pathway followed by an extrinsic caspase-8-dependent pathway [23]. CHIKV also exerts cytopathic activity through standard apoptosis machinery, in which it was shown that CHIKV releases viral proteins such as E1 and capsid, which shield into membrane vesicles. Engulfment of these CHIKV apoptotic blebs promotes the infection to the neighboring cells [23].

The cell and species specificity of SINV-induced cell death implies that cellular and viral regulators of apoptosis play important roles in determining the outcome of SINV infection. Nearly all vertebrate cell lines infected with SINVs do not survive after the infection. The mechanism by which CHIKV induced strong CPE in mammalian cells and weak CPE in mosquito cells is still not known. Apoptosis may be one of the reasons why CHIKV leads to cell death through strong CPE, because CHIKV induced strong apoptosis in Vero cells compared to C6/36 cells. Mosquito cells may carry apoptotic inhibitory genes.

Recently, virus-induced apoptosis mediated by an unfolded protein response (UPR) was hypothesized to be a crucial pathogenic event in viral infection: it creates conditions beneficial for an eventual viral infection. In general, newly synthesized secretory or membrane-bound

proteins are unable to fold properly in the endoplasmic reticulum (ER), leading to induction of ER stress and subsequent elicitation of UPR [24]. Dengue virus-infected mosquito cells continued growing, implying that an anti-ER stress factor might be involved in the process of viral replication in mosquito cells [25]. Mosquito cells trigger a pathway that protects infected cells from death, which might be how Aedes mosquitoes resist dengue virus infection [26]. Activation of the UPR to cope with ER stress in the early phase of viral infection was shown in various vertebrate cells [27, 28]. However, flavivirus-infected mammalian cells ultimately face apoptosis through the effects of ER stress [29].

In this paper, we reported that CHIKV induced strong CPE in Vero cells but light CPE in mosquito cells, which may be one of the reasons why mosquito can be a natural host of CHIKV without being killed. In the mosquito body, the genetic factors that govern susceptibility to CHIKV infection contribute to the weak CPE. Most of the C6/36 cells did not die after infection with CHIKV and became persistent, even after being passaged 20 times. The CHIKV virus could make adaptation in C6/36

cells, or mutant viruses might be released during the passages, which made the virus titers show a decreasing trend during passages. C6/36 cells can produce a higher titer of CHIKV than Vero cells.

Apoptosis is another attractive candidate antiviral response in mosquitoes, given its importance in other virus-host systems [30]. Therefore, the mosquito cell may carry some host factors against apoptosis. It would be interesting to clarify the differences in apoptosis mechanisms between Vero and C6/36 cells in CHIKV infection, as this may help us to understand the mechanisms of CHIKV-induced diseases in humans. Further study is needed to clarify the mechanisms.

Acknowledgements

References

1 Robinson MC: An epidemic of virus disease in southern province, Tanganyika territory, in 1952–1953. I. Clinical features. Trans R Soc Trop Med Hyg 1955;49:28–32.

2 McIntosh BM JPGaDSI: Rural epidemic of chikungunya in South Africa with involvement of Aedes (Diceromyia) furcifer (Edwards) and baboons. S Afr J Sci 1977;73:267–269.

3 Diallo M, Thonnon J, Traore-Lamizana M, Fontenille D: Vectors of chikungunya virus in Senegal: current data and transmission cycles. Am J Trop Med Hyg 1999;60:281–286.

4 Munasinghe DR, Amarasekera PJ, Fernando CF: An epidemic of dengue-like fever in Ceylon (chikungunya) – a clinical and haematological study. Ceylon Med J 1966;11:129–142.

5 Pavri K: Disappearance of chikungunya virus from india and south east asia. Trans R Soc Trop Med Hyg 1986;80:491.

6 Schwartz O, Albert ML: Biology and pathogenesis of chikungunya virus. Nat Rev Microbiol 2010;8:491–500.

7 Lumsden WH: An epidemic of virus disease in southern province, Tanganyika territory, in 1952–1953. II. General description and epidemiology. Trans R Soc Trop Med Hyg 1955; 49:33–57.

8 Pongsiri P, Auksornkitti V, Theamboonlers A, Luplertlop N, Rianthavorn P, Poovorawan Y: Entire genome characterization of chikungunya virus from the 2008–2009 outbreaks in Thailand. Trop Biomed 2010;27: 167–176.

9 Sourisseau M, Schilte C, Casartelli N, Trouillet C, Guivel-Benhassine F, Rudnicka D, Sol-Foulon N, Le Roux K, Prevost MC, Fsihi H, Frenkiel MP, Blanchet F, Afonso PV, Ceccaldi PE, Ozden S, Gessain A, Schuffenecker I, Verhasselt B, Zamborlini A, Saïb A, Rey FA, Arenzana-Seisdedos F, Despres P, Michault A, Albert ML, Schwartz O: Characterization of reemerging chikungunya virus. PLoS Pathog 2007;3:e89.

10 Solignat M, Gay B, Higgs S, Briant L, Devaux C: Replication cycle of chikungunya: a reemerging arbovirus. Virology 2009;393: 183–197.

11 Her Z, Malleret B, Chan M, Ong EK, Wong SC, Kwek DJ, Tolou H, Lin RT, Tambyah PA, Renia L, Ng LF: Active infection of human blood monocytes by chikungunya virus triggers an innate immune response. J Immunol 2010;184:5903–5913.

12 Karpf AR, Lenches E, Strauss EG, Strauss JH, Brown DT: Superinfection exclusion of alphaviruses in three mosquito cell lines persistently infected with sindbis virus. J Virol 1997;71:7119–7123.

13 Karpf AR, Blake JM, Brown DT: Characterization of the infection of Aedes albopictus cell clones by sindbis virus. Virus Res 1997; 50:1–13.

14 Brown DT: Alphavirus growth in cultured vertebrate and invertebrate cells; in Mayo MA, Herrop KA (eds): Vectors in Virus Biology. New York, Academic Press, 1984, pp 113–133.

15 Irusta PM, Lamos E, Galonek HL, Vander Maten MA, Boersma MC, Chen YB, Hardwick JM: Regulation of apoptosis by viruses that infect insects. Arch Virol Suppl 2004; 171–178.

16 Karpf AR, Brown DT: Comparison of sindbis virus-induced pathology in mosquito and vertebrate cell cultures. Virology 1998;240: 193–201.

17 Wang H, Blair CD, Olson KE, Clem RJ: Effects of inducing or inhibiting apoptosis on sindbis virus replication in mosquito cells. J Gen Virol 2008;89:2651–2661.

18 Dash PK, Tiwari M, Santhosh SR, Parida M, Lakshmana Rao PV: RNA interference mediated inhibition of chikungunya virus replication in mammalian cells. Biochem Biophys Res Commun 2008;376:718–722.